TEST TURBINE INSTRUMENTATION FOR CAVITY PURGE INVESTIGATIONS

Johan Dahlqvist **Jens Fridh** **Torsten H Fransson**
Heat and Power Technology,
KTH Royal Institute of Technology,
Stockholm, Sweden

ABSTRACT

The upstream wheelspace of the KTH Test Turbine has been instrumented with the aim of investigating cavity flow phenomena, as well as cavity-main annulus interaction. Measurements include static pressure, unsteady pressure and temperature.

The stage used is of high pressure steam turbine design. The trials include investigating the design point and also a high pressure, high speed operating point, assimilating gas turbine operation. At each point, varying amounts of purge flow are superposed and the influences on the measurements studied.

Initial results show considerable dependence of both operating point and amount of purge on the measurements.

INTRODUCTION

The optimization of secondary flows in turbomachines experiences increased relative importance as the main flow performance has been the focus of extensive research historically. This paper focuses on the instrumentation of the KTH Test Turbine for the purpose of investigation of wheelspace flows.

Purge of the wheelspace cavity is done in the gas turbine application to establish a temperature boundary between the hot main annulus flow and the interior of the annulus. This is essential to ensure the operation of the turbine, since an elevated temperature in these sensitive areas would lead to failure.

NOMENCLATURE

Symbol	Description	Definition
Greek		
ν	total-static isentropic velocity ratio	$=\frac{\Omega u}{\sqrt{2\Delta h_s}}$
Π	static-static pressure ratio	
Φ_0	sealing parameter	$=\frac{U}{\Omega b}$
Ω [rad/s]	rotor angular velocity	
Latin		
b [m]	hub radius	
m_g [kg/s]	main annulus mass flow rate	
m_c [kg/s]	purge flow rate	
N [rpm]	rotational speed	
s [m]	seal clearance	
U [m/s]	bulk mean radial velocity	$=\frac{m_c}{2\pi\rho bs}$
u [m/s]	rotor blade speed	
V [m/s]	flow velocity	
Abbreviations		
Cp	pressure coefficient	$=\frac{p-p_{ref}}{\frac{1}{2}\rho\Omega^2 b^2}$
cp [J/kgK]	specific heat	
MFR	mass flow ratio	$=\frac{m_c}{m_g+m_c}$
Subscripts		
φ	tangential coordinate	
r	radial coordinate	
s	static condition	
TC	thermocouple	

THE KTH TEST TURBINE

The Test Turbine at the Energy Department at KTH is an open-cycle test facility allowing investigation of turbine stages in a rotating environment. The rig operates at cool conditions, with air supplied by a 1 MW screw compressor. The flexibility of the rig allows for testing of up to 3 turbine stages, with a maximum air flow of 4.7 kg/s at 4 bar_a. The maximum speed of the rig is rated to 11 500 rpm. The maximum allowable stage tip diameter is 500 mm, while the minimum hub diameter is 280 mm.

The output power of the tested stages is measured through a torque meter mounted to the output shaft, featuring a torsional shaft. This power is finally dissipated by a water break. The facility has been modified and updated through the works of (Fridh 2012; Hushmandi 2010) among others.

STAGE 4B

Until now, the Test Turbine research has been focused to steam turbine applications. The stage in use is of high pressure steam turbine geometry, with a design point of low degree of reaction and low pressure ratio. The rotor is shrouded, with a positive hade angle, while the stator casing is meridionally profiled. Geometrical characteristics of stage 4B are presented in Table 1 (Mikaillian 2012). The geometry along with indicated flows is visible in Figure 1. The cavity geometry is of constant width, and covered from the main flow by a simple rim seal protruding from the stator side at the hub. The resulting gap ratio (axial separation to hub radius) is 0.022.

Table 1: Main geometric parameters of Stage 4B

	Stator	**Rotor**
Number of blades	42	58
Tip-to-hub ratio	1.149	1.192
Pitch-to-chord ratio	0.831	0.816
Aspect ratio	0.77	1.317

Through the work of this project, the focus is shifting toward the gas turbine application. This is done by operating the turbine at a higher pressure and a correspondingly higher rotational speed. In this paper, results for the stage design point as well as an elevated pressure ratio point are presented. The two operating points are summarized in

Table 2. To define the operating point, static to static pressure ratio is used in combination with isentropic velocity ratio, for a normalized speed as defined in the nomenclature. For the mass flow rate, both the mass flow ratio and Φ_0 as defined by (Sangan et al. 2013) is presented. The three levels of purge investigated for each operating point are referred to as zero, low and high purge respectively. The calculation of the flow density downstream of the stator is simplified by assuming an isentropic stator and using the upstream flow conditions.

ORIGINAL INSTRUMENTATION SETUP

The main measurement possibilities include total and static pressure taps as well as total temperature probes. These measurement points give the steady operating conditions, and are mainly concentrated to the main flow annulus. Steady measurement points are accompanied by output power measurement of the torque meter. Voltage signals and pressures are measured through multi-channel measurement processors and multi-channel pressure scanners respectively. The measurements are sent digitally to a PC operating LabView, which is used in monitoring and consolidating and the data into a unified output file. These measurements are sampled at a frequency in the order of 1 Hz where an average of about 100 points is used in defining an operating point once stable conditions are reached.

Table 2: Main operation parameters for the investigated points

Design Point			
Π	1.23		
v	0.48		
N	4450		
Φ_0	-0.024	0.049	0.104
MFR	-0.6%	1.3%	2.7%
Elevated Point			
Π	2.07		
v	0.61		
N	10520		
Φ_0	-0.015	0.043	0.082
MFR	-0.5%	1.5%	2.9%

One key advantage of the Test Turbine is the possibility of combining performance measurements of the current operating point with detailed flow field investigations. These investigations are mainly performed through pneumatic probe traverses. The traverse locations are positioned upstream and downstream of both rotor and stator. Using 5-hole conical probes, the flow features and loss distributions can be obtained in each section. Also traverse with seedgas concentration measurements and hot-wire are possible, to measure sealing effectiveness and turbulence intensity respectively. The traverse locations are indicated in Figure 1.

The stator disc is mounted to a hollow shaft, which can be rotated, allowing traverse in the tangential direction. It is also through this shaft that the purge flow is injected. In the current paper, the purge flow is bled from the main flow air supply.

NEW INSTRUMENTATION SETUP

The new measurement set, which is the focus of this paper, is located in the wheelspace upstream of the rotor. It consists of static pressure taps, total temperature thermocouples and rapid pressure transducers. These are placed on the stator-side of the cavity. The positions of the measurement points are displayed in Figure 2.

The purpose of the measurements is to quantify the cavity flow field in regard to flow swirl, seal performance and identification of rotating pressure instabilities, as described further in the following sections.

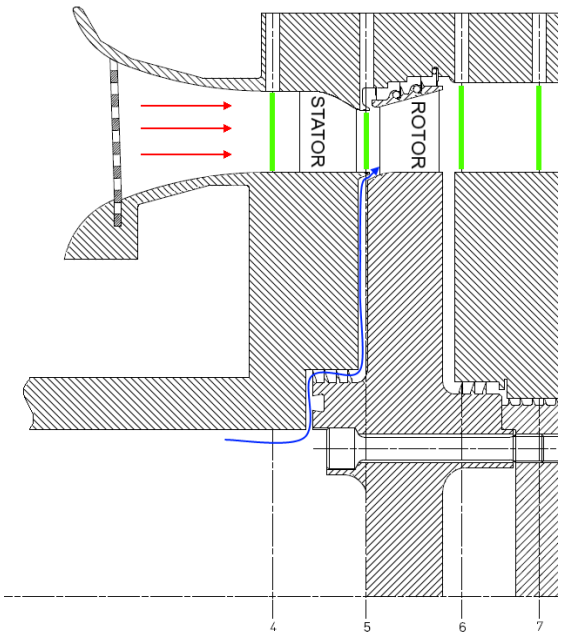

Figure 1: Simplified cross-section of stage 4B, with main flow indicated in red, the superposed purge flow in blue, and traverse planes in green.

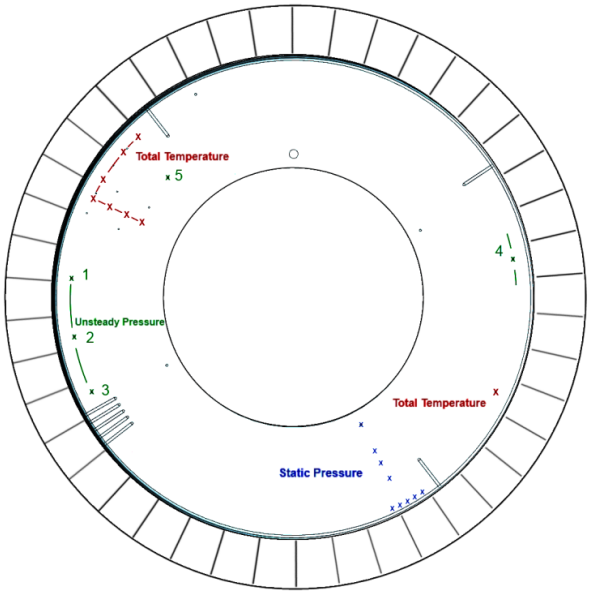

Figure 2: Sketched downstream view of the stator disc, indicating the positions of the implemented cavity measurements and numbering convention of the unsteady pressure transducers.

STATIC PRESSURE

Static pressure is measured through multi-channel pressure scanners with a measurement range of 69 kPa gauge. The static accuracy is 0.08% of the full scale with a 0.003% of full scale measurement resolution (Pressure Systems n.d.). The pressure scanners are re-zeroed to atmospheric pressure prior to experimental runs. The atmospheric component of the measured data is measured through an analog pressure transmitter with an accuracy of ±0.3 hPa (VAISALA 1997).

The static pressure taps are 0.6 mm in diameter, placed with the intention to cover the radial and tangential pressure distribution of the cavity. The radially positioned points are placed to make use of a previous tap at the lowest radius, and together cover the pressure distribution from the rotor shaft to the rim seal.

The intention of the radially distributed static pressure taps is to quantify the fluid swirl. As described by (Denton 1993), the velocity difference between two mixing flows, both in magnitude and direction, contributes to the losses associated with the mixing.

Figure 3 and Figure 4 show the radial distribution of the pressure coefficient, Cp_r, for the design and elevated point respectively. Here, the reference pressure is the value at the lowest radius tap. The radial position is normalized with respect to the hub radius.

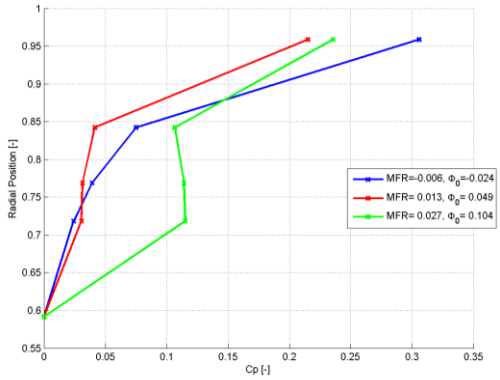

Figure 3: Cp_r at the stage design point, for three values of purge.

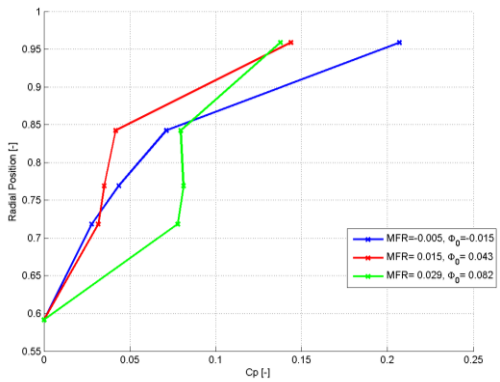

Figure 4: Cp_r at the elevated point, for three values of purge.

The tangentially distributed pressure taps are placed along one vane pitch. The intention of the measurement is an indication of where along the vane pitch ingress is most prone to occur.

For the tangential pressure coefficient, Cp_φ, the reference pressure used is the average main annulus

hub static pressure across one vane pitch. The pressure coefficient distribution below the seal is compared to the corresponding pressure coefficient in the main annulus. These measurements are taken on the stator hub, on the same axial position as the cavity measurement points.

Figure 5 and Figure 6 show the vane wake as a peak in the main annulus measurement. The difference between the curves indicates that ingress would be most likely to occur in the vane wake, where the static pressure is higher compared to the corresponding location in the cavity.

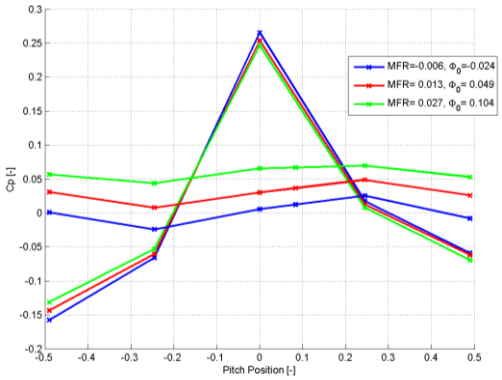

Figure 5: Cp_{φ} of main flow (peak) and under the rim seal, at the stage design point, for the three values of purge.

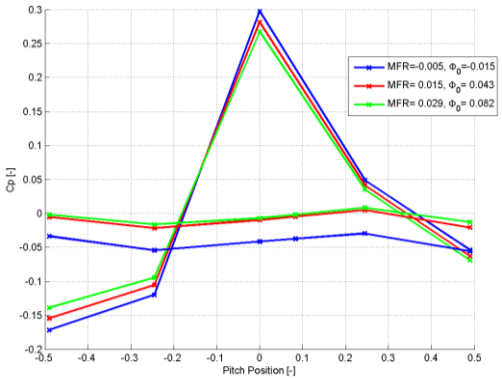

Figure 6: Cp_{φ} of main flow (peak) and under the rim seal, at the elevated operating point, for the three values of purge.

TOTAL TEMPERATURE

The cavity temperature distribution is measured through type K thermocouples, where the voltage is measured through a multi-channel measurement processor, with built-in temperature conversion and cold-junction measurement. The hardware sensitivity amounts to 0.02 °C (Measurement Systems Ltd 1996).

The temperature distribution in the cavity is measured by exposed thermocouple tips of 0.4 mm in diameter, protruding axially to the center of the cavity. The measurements are presented in Figure 7 and Figure 8, where the measured value is normalized with respect to inlet total temperature.

The main and purge flow are in these runs a split of the same air supply, implying that the significant temperature variation in the cavity for real gas turbine applications is not present. A temperature gradient changing with operating point and purge level is still visible. This gradient is thought to be due to variations in flow velocity in combination with influences of the surrounding.

The effect of velocity is normally compensated for using a recovery factor *r*, quantifying the proportion of the flow kinetic energy measured as total temperature, according to Equation 1.

$$T_{TC} = T_s + r\left(\frac{V^2}{2cp}\right) \qquad \text{Eq. 1}$$

Here, T_{TC} is the temperature measured by the thermocouple, while T_s is the static temperature of the fluid. For a shielded thermocouple, a high recovery factor is achieved, since stagnation is created around the measurement point. The recovery factor for an exposed tip as the ones used in this case can be compared to the unshielded thermocouples investigated by (Paniagua et al. 2002) where a recovery factors between 0.6 and 0.8 was obtained. However, when using this recovery factor in explaining the temperature difference between the cavity and the inlet temperature, it is obvious that the lower temperature measured in the cavity is not solely due to the recovery of the total condition. For the recovery factor set to 0.6 the residual velocity is higher than the rotor speed for the elevated zero purge case.

The additional factor suspected to be giving the lower temperature reading is the rotor being at lower temperature as a result of the cold outlet conditions. This would influence the thermocouple reading, mainly due to convection to the cavity region. The radiation effects are small at these temperature differences.

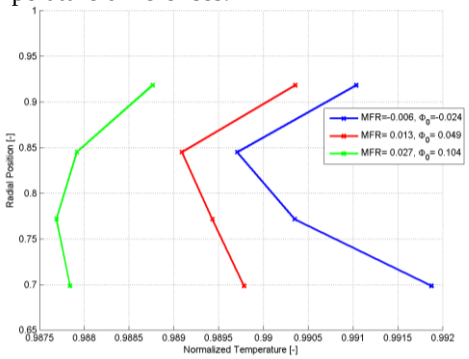

Figure 7: Normalized total temperature at the design point, for the three values of purge.

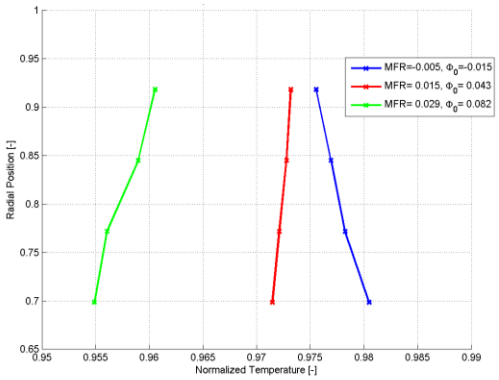

Figure 8: Normalized total temperature at the elevated operating point, for the three values of purge.

UNSTEADY PRESSURE

For the unsteady pressure measurements, miniature piezo-resistive 1.7 bar absolute pressure transducers are used. These are mounted flush with the stator wall surface. Here, three sensors have been placed with 15° separation on high radius. Diametrically opposite of this group is one sensor. An additional sensor is placed at lower radius in the cavity. The data is logged through a high-speed data acquisition system, which also provides the sensor excitation voltage of 5V.

A sampling frequency of 500 kHz is used, resolving a blade passing in 49 samples at the elevated point. This is however above the natural frequency of the sensor at 240 kHz. The absolute uncertainty of the sensors is 0.5% of full scale, resulting in 850 Pa (Kulite Semiconductor Products inc n.d.). The accuracy of measured pressure fluctuations and input frequencies is however much greater. Data is logged for 0.4 seconds at each operating point and purge condition.

The unsteady pressure data is coupled with the instantaneous rotational speed, which is closely monitored by a differential-hall-effect sensor. Each revolution triggers the sensor three times, where the sensor moves from low to high level within the laps of 4 samples (8 ns). The trigger time is interpolated from the time coordinate of the samples closest above and below a selected trigger level.

In all processing of the unsteady pressure data an integer number of revolutions are considered using the rpm data, to remove potential truncation errors. This data is also used in drawing the harmonics in the FFT representations.

The purpose of the sensors is to investigate rotating pressure structures in the cavity, comparable to the findings by (Jakoby et al. 2004). These pressure structures can induce vibrations in the shaft, affecting turbine lifetime, and also be the cause of unexpected hot-gas ingress.

The results are viewed through FFT of the signal data.

Figure 9 and
Figure 10 show the signal at blade passing frequency and the associated harmonics.

The influence of blade passes are more than an order of magnitude larger for the elevated case compared to design, when looking at one of the high-radius sensors. Also the harmonics are identified in the elevated case, contrary to design.

When doing a similar comparison for the first engine order and associated harmonics, an interestingly high influence of the fourth engine order is observed for the design point. This is not found for the elevated case, as seen in
Figure 11 and Figure 12 respectively.

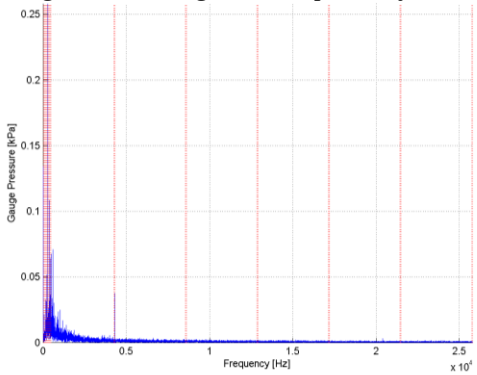

Figure 9: FFT of unsteady cavity pressure at design conditions, indicating blade passing frequency of 4297 Hz and 5 harmonics at sensor 1.

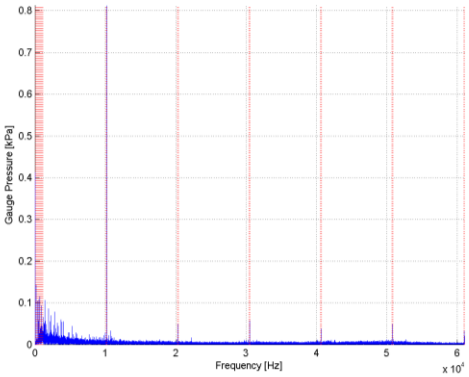

Figure 10: FFT of unsteady cavity pressure at elevated conditions, indicating blade passing frequency of 10170 Hz and 5 harmonics at sensor 1.

Upon addition of purge flow, the major changes are seen around the lower frequencies. In Figure 13 and Figure 14 purge is introduced at the design point, to compare to zero purge in
Figure 11. When previously the excitation was concentrated to the lower engine orders, the peaks are now shifted and not related to the engine orders. Hence, also the unsteady phenomena in the cavity are affected by the addition of purge flow. Similar tendencies are also seen for the elevated case.

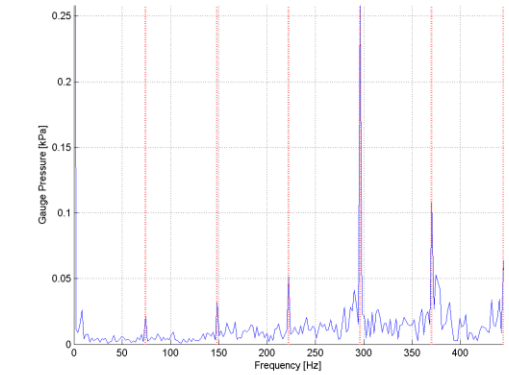

Figure 11: FFT of unsteady cavity pressure at design conditions, indicating 1EO frequency of 74 Hz and 5 harmonics at sensor 1.

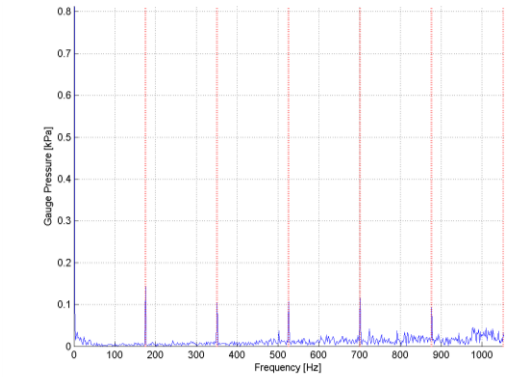

Figure 12: FFT of unsteady cavity pressure at elevated conditions, indicating 1EO frequency of 175 Hz and 5 harmonics at sensor 1.

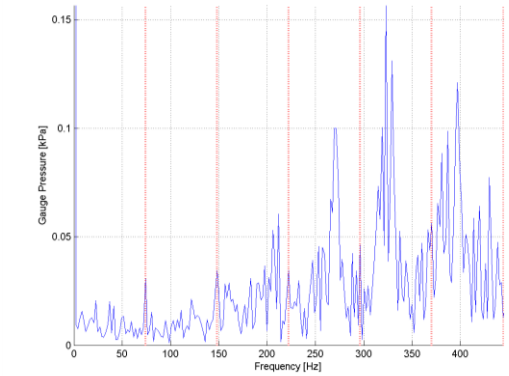

Figure 13: FFT of unsteady cavity pressure at design conditions, low purge, indicating 1EO frequency of 74 Hz and 5 harmonics at sensor 1.

Finally, the unsteady measurements are evaluated as an ensemble average. Here, the pressure data of all logged revolutions are combined, resulting in an average revolution signal. The revolutions are identified through the rpm sensor, and the corresponding pressure data is then resampled as to obtain a constant number of samples per revolution. Each sample is then averaged through the number of revolutions point-by-point.

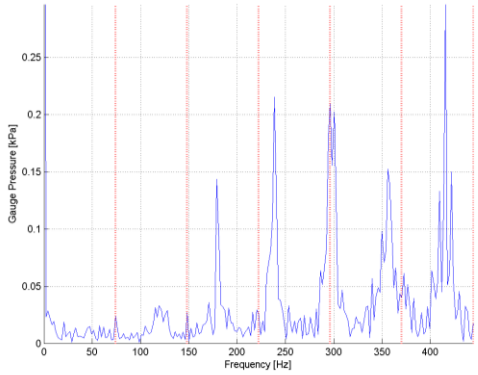

Figure 14: FFT of unsteady cavity pressure at design conditions, high purge, indicating 1EO frequency of 74 Hz and 5 harmonics at sensor 1.

The pressure coefficient is used here, where the reference pressure in this case is the DC component extracted from the FFT, bringing all curves to the same level. The angle difference between the sensors is compensated for in displaying the results, where the curve of each sensor is shifted for the angle position.

Figure 15 and Figure 16 show the ensemble average for the design point at zero and high purge respectively. In both cases the closely placed sensors 1, 2 & 3 show very similar reading. Sensor 5 is showing a lower level of excitation due to the lower radius position. For the zero-purge case, sensor 4 is showing some differences compared to the sensors on opposite diameter. In the high purge case however, the effect is magnified, showing half a wavelength difference in the observed fluctuations. Consequently, the signal being previously synchronized with the rotational speed is with the addition of purge changing through the revolution. This is an indication of pressure fluctuations as described by (Baumgartner et al. 1995) for the general case. The fluctuations are previously assumed to be due to their rotation, but may in fact also vary in magnitude with time.

For the elevated case, the blade passes dominate in the ensemble average and not the large scale fluctuations as in the design case. It can be seen in the construction of the ensemble averages that the method does not capture major pressure fluctuations, as seen in Figure 17 and Figure 18. Especially for the elevated case, the addition of purge leads to significant pressure fluctuations, while the resulting average mainly captures the blade passing frequency.

The frequency data visible in the completed ensemble average is of integer multiples of 1EO. Other fluctuations are effectively averaged out through the revolutions. In further evaluation of the data, the ensemble average should also be performed for important frequencies identified through the FFT analysis. This would be important due to the shift of frequencies in the purge case, as mentioned previously.

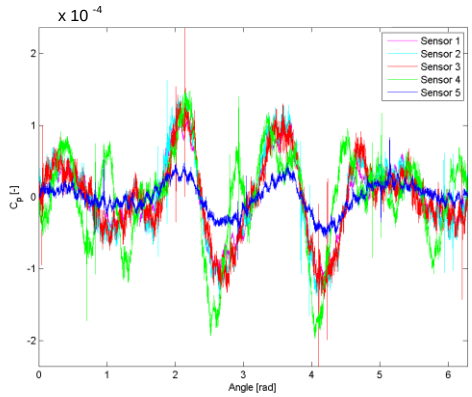

Figure 15: Pressure ensemble average at design point for zero purge.

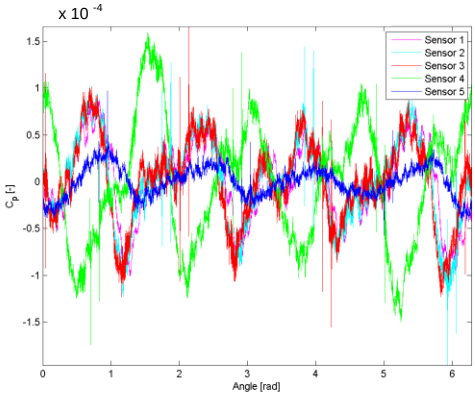

Figure 16: Pressure ensemble average at design point for high purge.

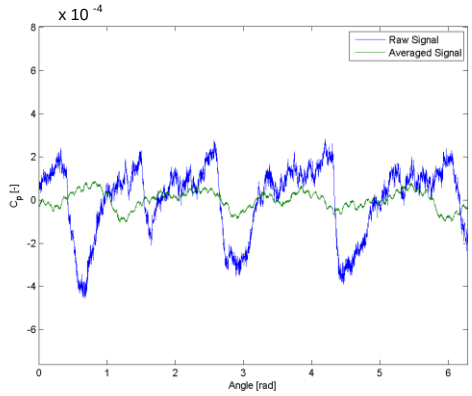

Figure 17: Ensemble construction comparing average with one revolution raw data for design, high purge.

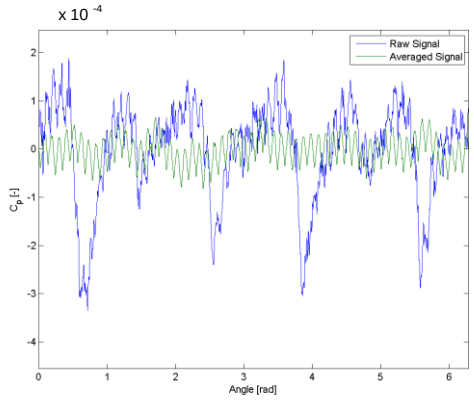

Figure 18: Ensemble construction comparing average with one revolution raw data for elevated, high purge.

CONCLUSIONS

The upstream cavity of the KTH Test Turbine has been successfully instrumented for investigation of cavity flow phenomena. Variations of the measured parameters are observed in respect to both purge rate and operating point. For the radial pressure distribution, an unexpected tendency is visible for the cases of superposed purge, where the measurements no longer agree with the radial balance which implies steady pressure increase with radius.

For the unsteady pressure measurements, the frequencies tend to shift with superposed purge, for both the design and elevated operating point. This is seen in both the FFT data and the ensemble average.

FUTURE WORK

Future work is planned both in evaluation of the current data and further measurement equipment upgrades. For evaluation, the fluid swirl ratio should be quantified, making use of the static pressure distribution. The temperature measurement in the cavity should be evaluated through a thermodynamic model, quantifying influence of conduction, radiation and fluid velocity. Also a calibration of the thermocouples' recovery factor is necessary.

In evaluating the origin of the frequencies associated with purge flow, cases with purge without stage rotation, and high amounts of purge during operation may be tested. This would exclude the influence of the main flow.

A high density purge flow supply is planned, for investigation of the effects of a significant density difference between purge flow and main flow. This addition would give a more significant temperature variation in the cavity, allowing for the temperature measurements to be used in quantifying main gas ingress. With a foreign gas, ingress and sealing performance will also be quantified by seedgas measurements in cavity and main annulus.

As the upgrades are put in place, the results will be correlated to the main annulus flow and stage performance.

ACKNOWLEDGMENTS

The current project in the KTH Test Turbine is performed through the Swedish research program Turbo Power, in cooperation with the Swedish Energy Agency and the industrial partners Siemens Industrial Turbomachinery and GKN Aerospace.

REFERENCES

Baumgartner, M., Kameier, F. & Hourmouziadis, J., 1995. Non-Engine Order Blade Vibration in a High Pressure Compressor by. In *Twelfth International Symposium on Airbreathing Engines*. Melbourne, pp. 1–13.

Denton, J.D., 1993. The 1993 IGTI Scholar Lecture: Loss Mechanisms in Turbomachines. *Journal of Turbomachinery*, 115(4), pp.621–656. Available at: http://dx.doi.org/10.1115/1.2929299.

Fridh, J., 2012. *Experimental Investigation of Performance , Flow Interactions and Rotor Forcing in Axial Partial Admission Turbines*. Stockholm: Royal Institute of Technology (KTH).

Hushmandi, N.B., 2010. *Numerical Analysis of Partial Admission in Axial Turbines*. Royal Institute of Technology (KTH).

Jakoby, R. et al., 2004. Numerical simulation of the unsteady flow field in an axial gas turbine Rim seal configuration. In *Proceedings of the ASME Turbo Expo 2004*. pp. 431–440. Available at: http://www.scopus.com/inward/record.url?eid=2-s2.0-10244224098&partnerID=tZOtx3y1.

Kulite Semiconductor Products inc, XCQ-062 Ultraminiature Pressure Transducer. Available at: http://www.kulite.com/docs/products/XCQ-062.pdf [Accessed July 11, 2014].

Measurement Systems Ltd, 1996. Datascan 8 / 16 Channel Measurement Processor. Available at: http://www.measurementsystems.co.uk/docs/722021C.PDF? [Accessed July 11, 2014].

Mikaillian, N., 2012. *Test turbine measurements and comparison with mean-line and throughflow calculations*. Royal Institute of Technology (KTH).

Paniagua, G., Dénos, R. & Oropesa, M., 2002. Thermocouple Probes for Accurate Temperature Measurements in Short Duration Facilities. In *Volume 2: Turbo Expo 2002, Parts A and B*. Amsterdam: ASME, pp. 209–217. Available at: http://www.scopus.com/inward/record.url?eid=2-s2.0-0037002779&partnerID=tZOtx3y1 [Accessed July 11, 2014].

Pressure Systems, 9010 Pneumatic Intelligent Pressure Scanner. , pp.1–8. Available at: http://www.a-tech.ca/doc_series/9010_Pneumatic_PScanner_ATI.pdf [Accessed July 11, 2014].

Sangan, C.M. et al., 2013. Experimental Measurements of Ingestion Through Turbine Rim Seals: Part 5 — Fluid Dynamics of Wheel-Space. In *Volume 3A: Heat Transfer*. ASME, p. V03AT15A003. Available at: http://www.scopus.com/inward/record.url?eid=2-s2.0-84890130655&partnerID=tZOtx3y1 [Accessed July 11, 2014].

VAISALA, 1997. PTB100 Series Analogue Barometer. Available at: https://www.eol.ucar.edu/isf/facilities/isff/sensors/vaisala/ptb100/PTB100.pdf [Accessed July 11, 2014].